Construction of Nanocrystalline Film on Nanowire Array *via* Swelling Electrospun Polyvinylpyrrolidone-Hosted Nanofibers for Use in Dye-Sensitized Solar Cells

Jih-Jen Wu,* Yan-Ru Chen, Wen-Pin Liao, Chun-Te Wu, and Chuh-Yung Chen

Department of Chemical Engineering, National Cheng Kung University, Tainan 701, Taiwan

ABSTRACT A 74% enrichment of the efficiency of ZnO nanowire (NW) dye-sensitized solar cells (DSSCs) is achieved by the addition of a novel light-scattering nanocrystalline film (nanofilm). The 100 nm thick nanofilm is derived from the polyvinylpyrrolidone-hosted SnO_2/ZnO nanofibers electrospun on the top of ZnO NW arrays *via* methanol vapor treatment followed by high-temperature calcination. Structural characterizations show that the film is composed of SnO_2 and ZnO nanocrystals with a diameter of ~10 nm. Short-circuit current, open-circuit voltage, and fill factor of the nanofilm/ZnO NW DSSCs are all superior to those of the ZnO NW DSSCs. The mechanism of photocurrent enhancement in the nanofilm/ZnO NW DSSCs has been investigated using optical modulation spectroscopy. Intensity modulation photocurrent spectroscopy (IMPS) measurements reveal that the dye-sensitized nanofilm does not contribute significant photocurrent in the nanofilm/ZnO NW DSSCs. The significant enhancement of the efficiency of the ZnO NW DSSCs is achieved by reflecting unabsorbed photons back into the NW anode using the novel light-scattering layer of nanofilm.

KEYWORDS: ZnO nanowire · dye-sensitized solar cell · electrospinning · nanofibers · nanofilms · light-scattering layer

Due to its low cost and high efficiency, dye-sensitized solar cell (DSSC) is a promising candidate to be a new renewable energy device.[1] The efficiency of a solar cell is determined by three factors of light-harvesting efficiency, electron injection efficiency, and electron collection efficiency. To attain a high light-harvesting efficiency, a dye-sensitized anatase TiO_2 nanoparticle (NP) film with high surface area is typically used to be the anode of the DSSC.[2] On the other hand, superior electron transport properties have been demonstrated by using single-crystalline ZnO nanowire (NW) DSSCs.[3,4] A higher electron collection efficiency compared to TiO_2 NP anode is achieved using the single-crystalline ZnO NW anode.[5] However, the photocurrents and the efficiencies of the ZnO NW cells are inferior to those of the conventional TiO_2 NP DSSCs.[3,5] It was suggested to be ascribed to insufficient surface area of the ZnO NW anode for dye adsorption.[3] To enlarge the surface area without sacrificing electron transport, composite anodes composed of high surface area NPs and a NW array have been demonstrated to improve the efficiency of ZnO NW DSSCs.[6−8]

Since there is considerable "free" space between NWs for light passing through, an alternative approach for improving the efficiency of NW DSSCs is to enhance the light-harvesting efficiency by reflecting unabsorbed photons back into the NW anode. In the case of the NP anode, a diffuse scattering layer composed of large colloids is utilized for this specific purpose of increasing light-harvesting efficiency.[9−11] The scattering effect depends on the refractive index, size, and position of the scattering particle. It is worth addressing that the sensitized scattering layers also directly contribute photoelectrons in aforementioned DSSCs. The mechanisms of the enhancements of photocurrents in these DSSCs have to be examined carefully.

Electrospinning of inorganic/polymer composite nanofibers has been demonstrated by mixing an inorganic sol−gel precursor with a water-soluble polymer solution.[12,13] A continuous gel network within the polymer matrix is produced in the electrospun composite nanofibers. Inorganic nanofibers can be subsequently obtained by calcination of the composite nanofibers at elevated temperatures in air for removing the polymer matrix.[12,13] Recently, electrospun TiO_2 and ZnO fibers have been demonstrated to be the anodes for dye sensitization in DSSCs.[14,15] In addition, fibers (~250 nm in diameter) electrospun on thick NP electrodes have been utilized as a light-harvesting layer, as well.[16]

*Address correspondence to wujj@mail.ncku.edu.tw.

Received for review June 7, 2010 and accepted September 07, 2010.

Published online September 14, 2010.
10.1021/nn101282w

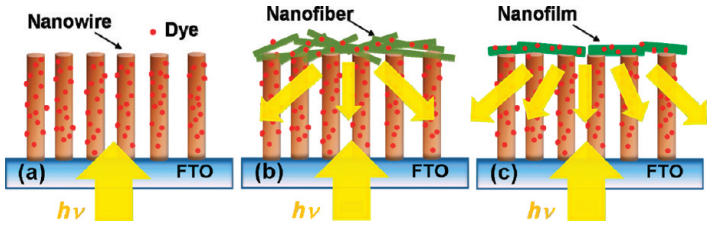

Figure 1. Schematics of (a) ZnO NW, (b) nanofiber/ZnO NW, and (c) nanofilm/ZnO NW anodes.

In order to reflect the lights passing through the free space between NWs back to the NW electrode portion, the light-scattering material in the NW DSSCs needs to exhibit a reflection index higher than that of the electrolyte which occupies the free space between NWs. The reflection indexes of the conventional electrolytes are ~1.4 in DSSCs. In addition, to examine the concept of the enhancement of the light-harvesting efficiency of NW DSSCs by the sole mechanism of reflecting unabsorbed photons back into the NW anode, the light-scattering layer which does not directly contribute photocurrent in the ZnO NW DSSCs is highly desired in the present work. To construct such "pure" light-scattering layer, one should employ a semiconductor material with lower conduction band edge compared to that of ZnO. The photoelectrons in the light-scattering layer, which inject from the adsorbed dye molecules, are therefore unable to efficiently transport to the ZnO NW anode. For aforementioned criteria, SnO_2 that possesses the reflection index of ~2.0[17] and the conduction band edge lower than that of ZnO[18] is the potential candidate for the light-scattering material in the ZnO NW DSSCs.

Due to its continuously one-dimensional and horizontal configuration, in the present work, the electrospun SnO_2/ZnO nanofibers are employed to be the light-scattering matter on the ZnO NW anode. The SnO_2/ZnO nanofibers, instead of pure SnO_2 nanofibers, are employed to improve the adhesion between the nanofibers and ZnO NWs. Moreover, by utilizing the polar-solvent-soluble characteristic of the polymer matrix,[12,13] a continuous nanofilm on the top of the ZnO NW array is obtained *via* methanol vapor treatment followed by a high-temperature calcination. The schematics of the nanofiber/ZnO NW and nanofilm/ZnO NW anodes are illustrated in Figure 1. A significant enrichment of the efficiency of ZnO NW DSSCs is achieved by the addition of the light-scattering nanofilm. The mechanism of photocurrent enhancement in the nanofilm/ZnO NW DSSCs has been investigated using optical modulation spectroscopy.

RESULTS AND DISCUSSION

Porous nanofibers composed of SnO_2/ZnO nanocrystals can be produced by the calcination of electrospun and polyvinylpyrrolidone (PVP)-hosted SnO_2/ZnO nanofibers (Figure S1, Supporting Information). High-density PVP-hosted SnO_2/ZnO nanofibers are further electrospun on the top of ZnO NW arrays to construct nanocomposite photoanodes for use in DSSCs. Figure 2a,b shows the top-view and cross-sectional scanning electron microscopy (SEM) images of the electrospun nanofibers on the ZnO NW array after calcination at 600 °C, respectively. A broad diameter distribution of the nanofibers on the ZnO NW array is observed in Figure 2a. The diameter of the PVP-hosted nanofiber increases slightly with time as a result of absorbing moisture by the polymer matrix of hydrophilic (polar-solvent-soluble) PVP[12,13] before calcination. The nanofibers electrospun earlier swell more than those electrospun later.

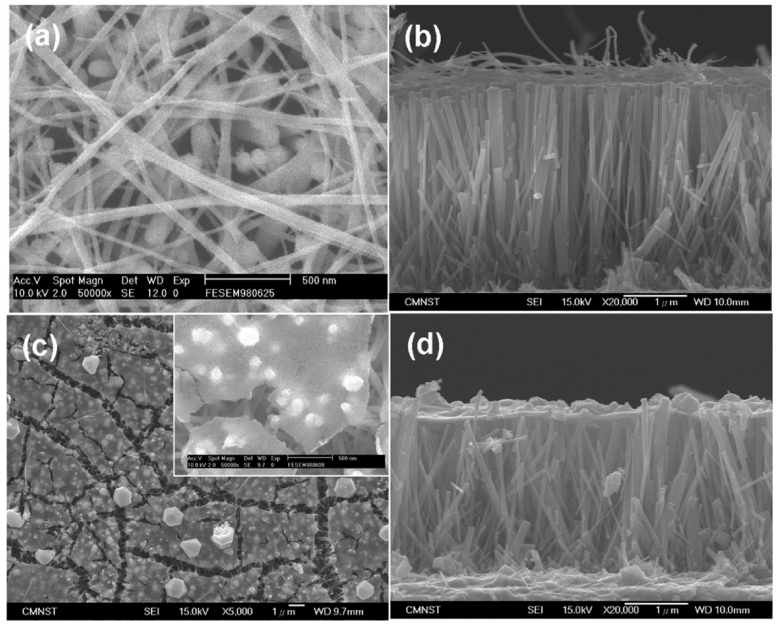

Figure 2. (a) Top-view and (b) cross-sectional SEM images of nanofibers on the ZnO NW array; (c) top-view and (d) cross-sectional SEM images of the nanofilm on ZnO NW array. The scale bar in the inset of (c) is 500 nm.

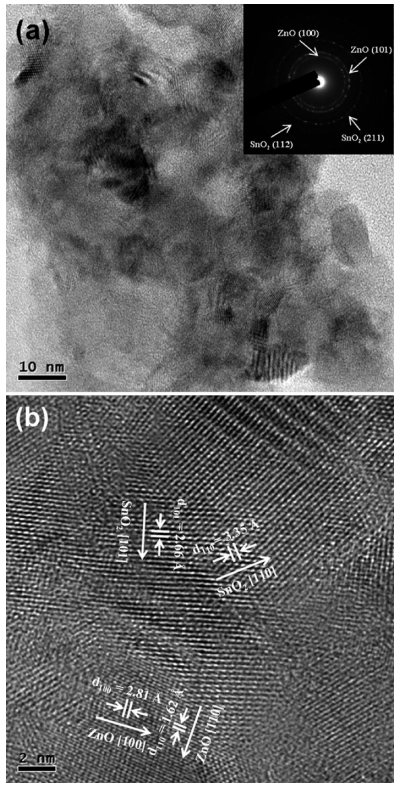

Figure 3. (a) TEM image and the corresponding SAED pattern (inset) of the nanofilm. (b) HRTEM image of the nanofilm.

Accordingly, in the present work, the hydrophilic characteristic of PVP is further employed to modify the feature of the light-scattering matter from the PVP-hosted nanofibers on the ZnO NW photoanode.

As-electrospun nanofibers on the ZnO NW array are treated in a methanol vapor ambiance at room temperature followed by calcination at 600 °C. Figure 2c,d displays typical top-view and cross-sectional SEM images of the nanocomposite with methanol vapor treatment, respectively. They reveal that a thin film instead of nanofibers is formed on the top of the ZnO NW array. Few particles with a size of ~1 μm also appear on the surface of the film. In addition, severe cracking of the thin film is observed, and the tips of the covered nanowires are embedded in the film, as shown in Figure 2c. Figure 2d shows that the thickness of the film is ~100 nm. We suggest that the as-electrospun nanofibers are reconstructed to a "free-standing" thin film *via* absorbing methanol vapor. The free-standing thin film, which is still composed of the inorganic sol dispersed in the PVP matrix, is supported by the tips of ZnO nanowires. After calination at 600 °C, PVP is decomposed away and a nanofilm with many cracks is thus formed on the top of the ZnO NW array. The structure of the nanofilm is further characterized by transmission electron microscopy (TEM). Typical TEM image and the corresponding selected area electron diffraction (SAED) pattern of the nanofilm are shown in Figure 3a and its inset. The TEM image reveals that the film is composed of nanocrystals with a diameter of ~10 nm. In addition, the *d* spacings calculated from the SAED patterns are consistent with those of hexagonal ZnO and tetragonal SnO_2 structures as indexed in the SAED pattern. Figure 3b reveals a typical high-resolution (HR) TEM image of the nanofilm. Lattice fringes are evidently shown, and the *d* spacings estimated from the HRTEM image can be referred to those of ZnO and SnO_2 crystals, as well.

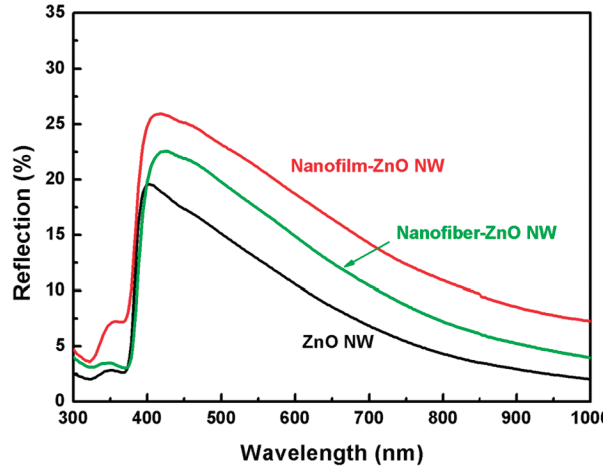

Figure 4. Reflection spectra of the ZnO NW array, nanofiber/ZnO NW array, and nanofilm/ZnO NW array on FTO substrates.

The reflection spectra of the ZnO NW array, nanofiber/ZnO NW array, and nanofilm/ZnO NW array formed on FTO substrates are shown in Figure 4. The three spectra illustrate the near band edge absorption of ZnO at 380 nm. In addition, Figure 4 reveals that the reflections of the three nanostructures are in order of ZnO NW array < nanofiber/ZnO NW array < nanofilm/ZnO NW array in the wavelength range of 400−1000 nm, demonstrating the reflective abilities of the nanofilm and nanofibers on the ZnO NW arrays. The lights reflected by the light-scattering nanofilm might experience multiple reflections in the free space between the nanofilm and FTO substrate, resulting in only an ~8% increase of the reflection compared to that of ZnO NWs.

D149, an indoline dye, is used to sensitize the nanofiber/ZnO NW array and nanofilm/ZnO NW array. It should be addressed here that the cracks of nanofilm, which permit electrolyte to penetrate into the ZnO NW array, make the nanocomposite of the nanofilm/ZnO NW array possibly be the anode of DSSC. Figure 5a shows the photocurrent density (*J*)−voltage (*V*) characteristics of the nanofiber/ZnO NW and nanofilm/ZnO NW DSSCs under the AM-1.5 illumination at 100 mW/cm^2. The *J*−*V* curve of ZnO NW DSSCs without the light-scattering layer is also illustrated in Figure 5a for comparison. The ZnO NW array is also annealed at 600 °C for use in the DSSC. The lengths of the NWs are ~3 μm for the fabrication of the three DSSCs. The 8 and 22% increments of the short-circuit current density (J_{sc}) of

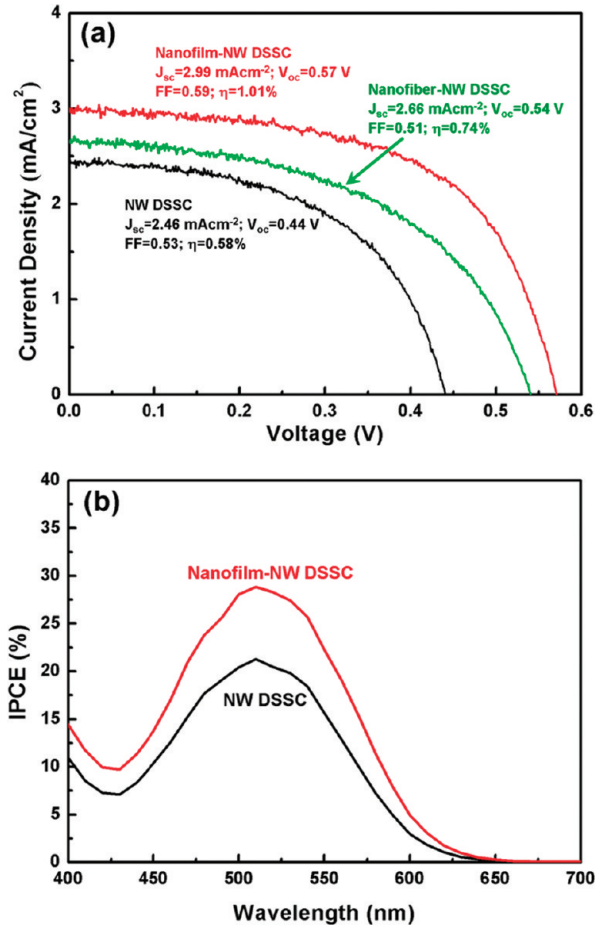

Figure 5. (a) *J*−*V* characteristics of the ZnO NW, nanofiber/ZnO NW, and nanofilm/ZnO NW DSSCs. (b) IPCE spectra of the nanofilm/ZnO NW and ZnO NW DSSCs.

ZnO NW DSSCs are achieved by forming nanofibers and nanofilm on the top of the ZnO NW anode, respectively, which are ascribed to the enhancement of the light-harvesting efficiency of the photoanode. A more significant enrichment of J_{sc} is achieved in the nanofilm/ZnO NW DSSCs as a result of the coverage of the nanofilm being larger than that of the nanofiber layer on the ZnO NW array, as shown in Figure 2a,c. In addition to the enrichment of J_{sc}, the open-circuit voltage (V_{oc}) and fill factor (FF) of ZnO NW DSSCs are also improved by the formation of nanofibers or nanofilm on the top of the ZnO NW anode. The increments of V_{oc} and FF in the nanofilm/ZnO NW DSSCs compared to the ZnO NW DSSCs are 29 and 11%, respectively. Combining the enhancements of J_{sc}, V_{oc}, and FF, a 74% improvement of the efficiency (η) of the ZnO NW is achieved by the addition of the light-scattering nanofilm. Figure 5b illustrates the IPCE spectra as a function of wavelength for the nanofilm/ZnO NW and ZnO NW DSSCs. The nanofilm/ZnO NW DSSC shows a superior photoelectrical response to ZnO NW DSSCs in the wavelengths ranging from 400 to 650 nm.

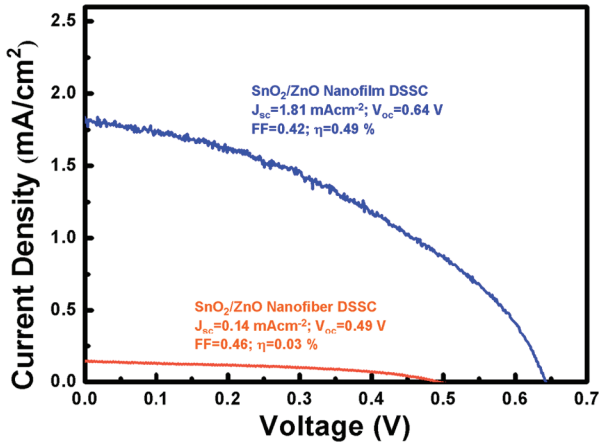

Figure 6. *J*−*V* characteristics of the SnO_2/ZnO nanofiber and SnO_2/ZnO nanofilm DSSCs.

SnO_2/ZnO nanofiber and SnO_2/ZnO nanofilm DSSCs are further fabricated to examine the photovoltaic properties of the nanofiber and nanofilm DSSCs in the absence of the ZnO NWs. Typical top-view and cross-sectional-view SEM images of the SnO_2/ZnO nanofibers and nanofilms on FTO substrates are shown in Figure S2 (Supporting Information), revealing similar features to those formed on ZnO NW arrays as displayed in Figure 2. Figure 6 shows the *J*−*V* characteristics of the SnO_2/ZnO nanofiber and nanofilm DSSCs under the AM-1.5 illumination at 100 mW/cm^2. The SnO_2/ZnO nanofiber DSSC possesses rather low J_{sc} and η, which may result from the poor interface between nanofibers and FTO substrate. On the other hand, with a film thickness of ~100 nm, the SnO_2/ZnO nanofilm DSSC performs as an efficient solar cell with the J_{sc} and η of 1.81 mA cm^{-2} and 0.49, respectively.

V_{oc} is fundamentally corresponding to the difference of the Fermi level of anode and the redox potential of electrolyte.[19] With nanofibers or nanofilm on the top of ZnO NW anode, the higher concentration of photoelectron on the conduction band, that is, larger photocurrent as shown in Figure 5a, elevates the quasi-Fermi level of the ZnO NW anode, which could result in larger V_{oc} in the nanofiber/ZnO NW and nanofilm/ZnO NW DSSCs. On the other hand, we can not rule out other influences of the SnO_2/ZnO nanofilm on the V_{oc} of nanofilm/ZnO NW DSSC since the V_{oc} of nanofilm DSSC is considerably larger than that of the ZnO NW cell. There are two possible mechanisms for the improvement of light-harvesting efficiency by the nanofibers and nanofilm on the top of ZnO NW anode. One is that the surface area of the anode is increased by the addition of nanofibers or nanofilm, which results in a higher amount of dye adsorption and therefore higher J_{sc}. The other one is that the nanofibers and nanofilm perform as the light-scattering matter on the top of ZnO NW anodes to enhance light-harvesting efficiency. Since the nanofibers and nanofilm are composed of SnO_2/ZnO nanocrystals and the conduction band minimum of SnO_2 is lower than that of ZnO,[18] the photoelectrons injected into the nanofibers and nanofilm are unable to efficiently transport to the ZnO NW anode.

Although the SnO_2/ZnO nanofilm DSSC demonstrates an apparent J_{sc}, we suggest that J_{sc} values in the nanofiber/ZnO NW and nanofilm/ZnO NW DSSCs are mainly attributed to the photoelectrons excited from the dye molecules adsorbed on the single-crystalline ZnO NW array. That is, the major role of the nanofibers and nanofilm is the light-scattering matter on the top of the ZnO NW anode. Further investigation of the mechanism of photocurrent enhancement is performed by optical modulation spectroscopy.

Intensity modulation photocurrent spectroscopy (IMPS) is employed to measure the dynamic of electron transport in the ZnO NW, nanofiber/ZnO NW, and nanofilm/ZnO NW DSSCs. Light intensity dependence of dynamics of electron transport in the three DSSCs obtained from IMPS measurements are shown in Figure 7. IMPS measurements reveal that the ZnO NW DSSC sustains a constant transit time of 52 μs when the light intensity is decreased. The constant transit time of the ZnO NW DSSC has been demonstrated, and it is ascribed to very few traps existing in the ZnO NWs.[5,20] On the other hand, the electron transit times in the nanofiber/ZnO NW and nanofilm/ZnO NW DSSCs keep constants of 514 and 527 μs, respectively, when the light intensity is varied. The constant transit times indicate that electrons experience very few trapping/detrapping events as well when diffusing through the nanofiber/ZnO NW and nanofilm/ZnO NW anodes. However, many traps exist within the grain boundaries of light-scattering layers since both nanofibers and nanofilm are composed of nanocrystals, as shown in Figure S1 (Supporting Information) and Figure 3. The electron transport properties in the SnO_2/ZnO nanofilm DSSC (in the absence of the ZnO NW array) is further examined by IMPS. The behavior of the light intensity dependence on the electron transit time in the SnO_2/ZnO nanofilm DSSC is also shown in Figure 7, revealing the significantly larger transit times than that in the nanofilm/ZnO NW anode. Moreover, the decrease of the transit time in the nanofilm anode is observed as increasing the light intensity. It results from the fact that, with a higher light intensity, more photoelectrons are present to fill the deep traps of the nanofilm anode and electron trapping/detrapping involves shallower trap levels only.

According to the IMPS results of the SnO_2/ZnO nanofilm DSSC, an increase of the transit time will be observed in the nanofiber/ZnO NW or nanofilm/ZnO NW DSSCs as decreasing the light intensity if there was significant photocurrent originated from the dye-sensitized nanofibers or nanofilm on the top of ZnO NW arrays. However, the constant electron transit times are obtained in the nanofiber/ZnO NW and nanofilm/ZnO NW DSSCs under various light intensities. In addition, the transit time in the nanofilm/ZnO NW DSSCs is significantly shorter than those in the SnO_2/ZnO nanofilm DSSCs. The results indicate that the light-scattering layers of nanofibers and nanofilm do not contribute significant photocurrent in the nanofiber/ZnO NW and nanofilm/ZnO NW DSSCs. We suggest that the apparently larger electron transit times in nanofiber/ZnO NW and nanofilm/ZnO NW DSSCs compared to that in the ZnO NW DSSC are ascribed to reflection phase shifts of the lights reflected/scattered by the light-scattering layer during IMPS measurement (Supporting Information). Unlike the conventional light-scattering layers, which not only reflect light but also directly contribute photocurrent in DSSCs, in the present work, the nanofibers and nanofilm play a major role in light scattering in the nanostructured ZnO NW DSSCs. It is therefore concluded that the considerable enhancement of the efficiency of the ZnO NW DSSC is achieved by reflecting unabsorbed photons back into the NW anode using the novel light-scattering layer of nanofilm.

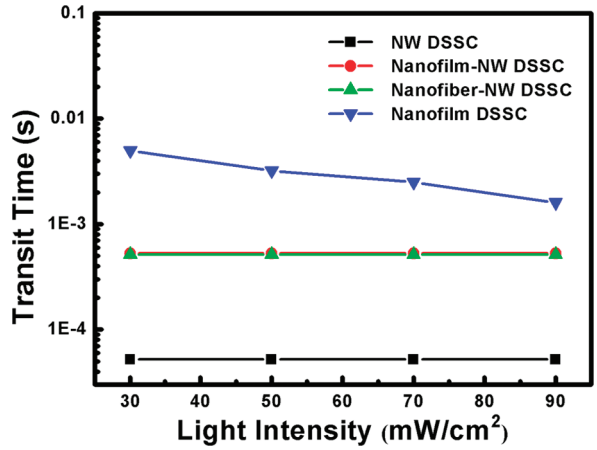

Figure 7. Light intensity dependence of the transit times in the ZnO NW, nanofiber/ZnO NW, nanofilm/ZnO NW, and nanofilm DSSCs.

CONCLUSIONS

A 74% enrichment of the efficiency of ZnO NW DSSC is achieved using a novel light-scattering layer of nanofilm. To construct a nanofilm on a ZnO NW array, the PVP-hosted SnO_2/ZnO nanofibers electrospun on the top of NWs are swollen using methanol vapor followed by high-temperature calcination. Structural characterizations show that the film is composed of SnO_2 and ZnO nanocrystals with a diameter of ~10 nm. J_{sc}, V_{oc}, and FF of the nanofilm/ZnO NW DSSCs are all enhanced compared to those of the ZnO NW DSSCs. The reflection measurements confirm the reflective ability of the nanofilm on the top of ZnO NW arrays. IPCE spectra also show that the nanofilm/ZnO NW DSSC possesses a superior photoelectrical response to ZnO NW DSSC. The IMPS results show a constant but apparently larger electron transit time in the nanofilm/ZnO NW DSSCs compared to that in the ZnO NW cell under various light intensities, which indicates that the dye-sensitized nanofilm does not contribute significant photocurrent in the nanofilm/ZnO NW DSSC. The significant enhance-

ment of the efficiency of the ZnO NW DSSC by the light-scattering layer of nanofilm is mainly attributed to the successful reflection of unabsorbed photons back into the NW anode.

EXPERIMENTAL METHODS

Formation of ZnO NW arrays on fluorine-doped tin oxide (FTO) substrates has been described in detail elsewhere.[8] The lengths of the NWs are ~3 μm for the fabrication of DSSCs. Polymer-hosted SnO_2/ZnO nanofibers were directly electrospun onto the collector or ZnO NW array using a methanolic solution of 0.15 g/mL polyvinylpyrrolidone (PVP, M_w = 1 300 000, Aldrich), 0.1 M $ZnAc_2 \cdot 2H_2O$, 0.05 M $SnCl_4 \cdot 5H_2O$, and 1.3 M *tert*-butylamine (TBA). An electrical potential of 15 kV was applied across the syringe and collector with a distance of 9 cm. SnO_2/ZnO nanofibers were obtained after the calcination of PVP-hosted nanofibers at 600 °C for 1 h. To construct the SnO_2/ZnO nanofilm on the top of ZnO NW array, as-electrospun nanofibers on the ZnO NW array were treated in a methanol vapor ambiance at room temperature for 10 min followed by calcination at 600 °C for 1 h. The morphologies of the nanostructures were examined using SEM (JEOL JSM-7000F). The crystal structures of the nanofibers and nanofilms were investigated using XRD (Rigaku D/MAX-2000 and Rigaku D/MAX-2500) and TEM (JEOL 2100F). Optical reflectance of the nanostructures were measured using a UV−vis−NIR spectrophotometer (JASCO V-670) equipped with an integrating sphere. The incident light enters from FTO glass into the nanostructures.

D149 dye (Mitsubishi Paper Mills, Ltd.) was used to sensitize the ZnO-based electrodes. Dye adsorption was carried out by immersing the anode in a 1×10^{-5} M acetonitrile/*t*-butyl alcohol (1:1) solution of D149 at 80 °C for 1 h. The sensitized electrode and platinized FTO counter electrodes were sandwiched together with 25 μm thick hot-melt spacers (SX 1170-25, Solaronix SA). Liquid electrolyte solutions composed of 0.5 M Pr_4NI and 50 mM I_2 in a 1:4 volume ratio of ethylene carbonate and acetonitrile were employed for the D149-sensitized DSSCs. Photovoltaic characteristics of the DSSCs were measured under AM-1.5 simulated sunlight at 100 mW cm^{-2} (300 W, Model 91160A, Oriel). The exposed area is 0.16 cm^2 for all cells.

IMPS measurements were performed under a modulated green LED light (530 nm) driven by a source supply (Zahner, PP210) and a potentiostat (Zaher, IM6ex) with a frequency response analyzer (FRA). The illumination intensity ranged from 30 to 90 mW cm^{-2}. The light intensity modulation was 20% of the base light intensity over the frequency range of 10^{-1}−10^4 Hz. The amplitudes and phase shifts of the modulated short-circuit photocurrents relative to the modulated illumination were measured by FRA by combining the signals from PP210 and IM6eX for IMPS. The method for extraction of transit times of the DSSCs from the IMPS responses has been described in detail elsewhere.[5]

Acknowledgment. Financial support from the National Science Council and the Bureau of Energy, Ministry of Economic Affairs in Taiwan under Contract No. NSC 96-2628-E006-017-MY3 and 98-D0204-2, respectively, is gratefully acknowledged.

Supporting Information Available: Characterization of SnO_2/ZnO nanofibers prepared by electrospinning, SEM images of nanofibers and nanofilm on FTO substrates, and possible reason for the significant increase of constant transit times in the nanofilm/ZnO NW DSSC. This material is available free of charge *via* the Internet at http://pubs.acs.org.

REFERENCES AND NOTES

1. Grätzel, M. Recent Advances in Sensitized Mesoscopic Solar Cells. *Acc. Chem. Res.* **2009**, *42*, 1788–1798.
2. Barbe, C. J.; Arendse, F.; Comte, P.; Jirousek, M.; Lenzmann, F.; Shklover, V.; Grätzel, M. Nanocrystalline Titanium Oxide Electrodes for Photovoltaic Applications. *J. Am. Ceram. Soc.* **1997**, *80*, 3157–3171.
3. Law, M.; Greene, L. E.; Johnson, J. C.; Saykally, R.; Yang, P. D. Nanowire Dye-Sensitized Solar Cells. *Nat. Mater.* **2005**, *4*, 455–459.
4. Galoppini, E.; Rochford, J.; Chen, H. H.; Saraf, G.; Lu, Y. C.; Hagfeldt, A.; Boschloo, G. Fast Electron Transport in Metal Organic Vapor Deposition Grown Dye-Sensitized ZnO Nanorod Solar Cells. *J. Phys. Chem. B* **2006**, *110*, 16159–16161.
5. Wong, D. K.-P.; Ku, C.-H.; Chen, Y.-R.; Chen, G.-R.; Wu, J.-J. Enhancing Electron Collection Efficiency and Effective Diffusion Length in Dye-Sensitized Solar Cells. *ChemPhysChem* **2009**, *10*, 2698–2702.
6. Baxter, J. B.; Aydil, E. S. Dye-Sensitized Solar Cells Based on Semiconductor Morphologies with ZnO Nanowires. *Sol. Energy Mater. Sol. Cells* **2006**, *90*, 607–622.
7. Ku, C.-H.; Wu, J.-J. Electron Transport Properties in ZnO Nanowire Array/Nanoparticle Composite Dye-Sensitized Solar Cells. *Appl. Phys. Lett.* **2007**, *91*, 093117.
8. Ku, C.-H.; Wu, J.-J. Chemical Bath Deposition of ZnO Nanowire−Nanoparticle Composite Electrodes for Use in Dye-Sensitized Solar Cells. *Nanotechnology* **2007**, *18*, 505706.
9. Rothenberger, G.; Comte, P.; Grätzel, M. A Contribution to the Optical Design of Dye-Sensitized Nanocrystalline Solar Cells. *Sol. Energy Mater. Sol. Cells* **1999**, *58*, 321–336.
10. Hore, S.; Vetter, C.; Kern, R.; Smit, H.; Hinsch, A. Influence of Scattering Layers on Efficiency of Dye-Sensitized Solar Cells. *Sol. Energy Mater. Sol. Cells* **2006**, *90*, 1176–1188.
11. Zheng, Y.-Z.; Tao, X.; Wang, L.-X.; Xu, H.; Hou, Q.; Zhou, W.-L.; Chen, J.-F. Novel ZnO-Based Film with Double Light-Scattering Layers as Photoelectrodes for Enhanced Efficiency in Dye-Sensitized Solar Cells. *Chem. Mater.* **2010**, *22*, 928–934.
12. Li, D.; Xia, Y. Electrospinning of Nanofibers: Reinventing the Wheel. *Adv. Mater.* **2004**, *16*, 1151–1170.
13. Greiner, A.; Wendorff, J. H. Electrospinning: A Fascinating Method for the Preparation of Ultrathin Fibres. *Angew. Chem., Int. Ed.* **2007**, *46*, 5670–5703.
14. Song, M. Y.; Kim, D. K.; Ihn, K. J.; Jo, S. M.; Kim, D. Y. Electrospun TiO_2 Electrodes for Dye-Sensitized Solar Cells. *Nanotechnology* **2004**, *15*, 1861–1865.
15. Zhang, W.; Zhu, R.; Liu, X.; Liu, B.; Ramakrishna, S. Facile Construction of Nanofibrous ZnO Photoelectrode for Dye-Sensitized Solar Cell Applications. *Appl. Phys. Lett.* **2009**, *95*, 043304.
16. Chuangchote, S.; Sagawa, T.; Yoshikawa, S. Efficient Dye-Sensitized Solar Cells Using Electrospun TiO_2 Nanofibers as a Light Harvesting Layer. *Appl. Phys. Lett.* **2008**, *93*, 033310.
17. Lide, D. R. *CRC Handbook of Chemistry and Physics*, 76th ed.; CRC Press: NewYork, 1995; pp 4−133.
18. Thavasi, V.; Renugopalakrishnan, V.; Jose, R.; Ramakrishna, S. Controlled Electron Injection and Transport at Materials Interfaces in Dye Sensitized Solar Cells. *Mater. Sci. Eng. R* **2009**, *63*, 81–99.
19. Peter, L. "Sticky Electrons" Transport and Interfacial Transfer of Electrons in the Dye-Sensitized Solar Cell. *Acc. Chem. Res.* **2009**, *42*, 1839–1847.
20. Martinson, A. B. F.; McGarrah, J. E.; Parpia, M. O. K.; Hupp, J. T. Dynamics of Charge Transport and Recombination in ZnO Nanorod Array Dye-Sensitized Solar Cells. *Phys. Chem. Chem. Phys.* **2006**, *8*, 4655–4659.